Plasmonic heterostructures for sensing applications

Author: Marc Martínez Castells.
*Facultat de Física, Universitat de Barcelona, Diagonal 645, 08028 Barcelona, Spain.**

Advisors: Amílcar Labarta Rodríguez
(Dated: February 5, 2021)

Abstract: We present a study of the optical response of an array of plasmonic nanoelements on top of a two-dimensional photonic crystal. The excitated collective plasmons together with the role of the photonic crystal that intensifies their excitation give rise to a particularly interesting electric field distribution. These properties, which have been optimized by tuning the heterostrucutre parameters, are specially suitable to design a sensor of refractive index changes. Using numerical simulations, we study the behavior of our basis heterostructure and its response when the test material is put in contact with the system. The study evidences the high efficiency of the heterostructure, whose properties result in a sensitivity of the sensor so much higher than that obtained in other similar sensors.

I. INTRODUCTION

Plasmonics is one of the most active branches of research within the field of nanophotonics. The object of study are surface plasmons, which can be defined, in broad terms, as the collective oscillations of the conduction electrons contained in a metal laying at the interface with a dielectric material due to the interaction of these with impinging electromagnetic radiation.

Depending on how the excitation of surface plasmons is, known as Surface Plasmon Resonance (SPR), two classes can be established: Surface Plasmon Polaritons (SPP) and Localized Surface Plasmons (LSP) [1].

The first ones are excited when electromagnetic radiation of suitable frequency and wavelength reaches an interface that separates a dielectric and a metallic media. The originated propagating wave involves both charge oscillation in the metal and an evanescent electromagnetic field in the dielectric [2].

On the other hand, LSP are non-propagating oscillations generated when electromagnetic radiation reaches a metallic nanostructure smaller or in the order of the wavelength of the incident radiation. These are coupled excitations of the conduction electrons with local oscillations of the electromagnetic field. The origin of the oscillations is in the recovery force generated when the waves affect the electrons and these move from their equilibrium position. The non-propagating behavior of LSP implies their excitation only calls for an adequate frequency (known as resonance frequency) in the incident wave. This is in contrast to SPP, for which the wave vector must also be matched which is hard to achieve. LSP will be thus used in this project.

Studying LSP excitacions, we can differentiate between two modes. The first one is a local mode originated by the near-field coupling between nearest neighboring metallic nanostructures (for instance, dipolar polarization) known as Localized Surface Resonances (LSR). An example of LSR is shown in Fig. 2(a).

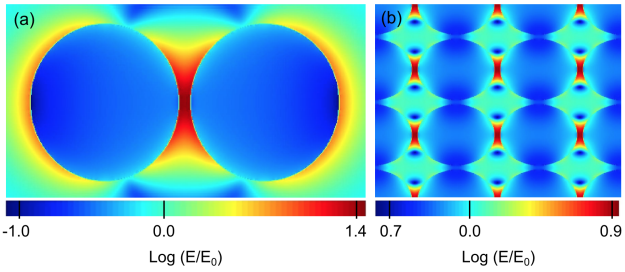

FIG. 1: Simulations of the distributions of the magnitude of the electric field in comparison with the incident electric field E_0 for a LSR mode appearing between two neighboring Au disks (a) and a SLR mode for a square array of the same disks (b).

These excitations occur at low energies, so that their corresponding peaks in the excitation spectrum appear in the infrared and are associated with areas of strong confinement of the electromagnetic field between each pair of facing nanostructures (known as hot-spots) that implies a large enhancement of the amplitude of the evanescent electric field.

The second mode, Surface Lattice Resonance (SLR), for which an example it is shown in Fig. 2(b), typically appears when the nanostrucures are arranged into a two-dimensional ordered lattice whose period is comparable to the wavelength of the incident radiation. It has a collective origin in which each excited plasmon of the array interacts with the rest giving rise to a constructive interference. Therefore, SLR is a coupled excitacion of the LSP of the array that is associated with several outstanding phenomena used in a wide range of applications.

For instance, the SLR mode presents notable narrowing of the resonance width (compared with LSR) [3]. Moreover, despite being less intense, it is the cause of a non-local enhancement of the electric field throughout

*Electronic address: mmartica176.alumnes@ub.edu

the whole surface of the array that, in some special cases, might be pointing along the normal direction to the surface. This will be the case of the heterostructure studied in this work. These properties will bring higher sensitivity to the structure so that the system will present a remarkable response for sensing aims [4].

The process of light scattering involved in SLR is explained by the diffraction condition of a two-dimensional array of nanostructures. Should a beam of monochromatic light reach a periodic lattice, the emerging waves will interfere constructively when the path difference is an integer multiple of the wavelength: $d\cos\theta = m\lambda$, where d is the distance between two adjacent lines containing equivalent lattice points, θ is the angle of incidence measured from the perpendicular to the plane, m is a natural number that gives the order of the diffraction peak, and λ is the wavelength of the incident radiation. Then, for normal incidence of the radiation, the first diffraction resonance of the lattice will be located at $\lambda = d$. As it can be deduced, another advantage of SLR is that just by varying the lattice constant the peaks can be obtained wherever it is needed.

In addition, the metallic nanostructure lattice is normally placed on top of a dielectric substrate (typically silica) that can be nanostructured in the same manner as the plasmonic system. Accordingly, apart from plasmonic excitations, it is important to introduce this kind of strucure known as a photonic crystal [5]. This type of crystal is formed by two different refractive-index materials set out in a periodic form. When the light propagates inside the structure it will be scattered by a periodic distribution of two materials with different refractive index causing a spatial rearrengement of the radiation intensity when the Bragg condition is fulfilled. When the difference between the refractive-indexes is big enough, the range of frequencies to which there are no modes of propagation is defined as bandgap. At both sides of this region, two diffraction modes corresponding to standing waves inside the system appear: the high-frequency mode which condenses the electromagnetic wave in the low-refractive-index material and the low-frequency one which concentrates it in the high-refractive-index material. This confinement of the field energy gives rise to local field enhancement, which will intensify the diffraction peaks of the metal themselves and can be used to enhance optical effects and manipulate the spatial distribution of an electromagnetic field in the near-field region. These properties of modulation and enhancement of the electric field will be used in the project by taking advantage of the coupling between the modes of the plasmonic array and the photonic crystal.

All in all, in this work, we will study the optical response of illuminating a plasmonic heterostructure formed by a metallic layer where a periodic structure is carved by removing the metal from specific areas that form an ordered pattern and underneath a photonic crystal with exactly the same periodic structure. As a consequence, we will be exciting the cloud of delocalized electrons of the metal giving rise to SLR and will be obtaining collective modes inside both the metal layer and the photonic crystal. All these excitations, whose coupling will be used to get a better optical response of the metal, and which will give rise to narrow diffraction peaks, will create a strong enhancement of the electric field. Once we have characterized and understood our system behavior, our objective will be to detect a thin layer of a test material placed above the metal by analyzing the optical response changes, such as the diffraction peak positions.

II. STRUCTURE AND SIMULATIONS

In order to study the optical response of the system we have made use of the Finite-Difference Time-Domain (FDTD) method within Lumerical's software [6], which works calculating the evolution of electromagnetic waves by discretizing and solving Maxwell's equations from their time-dependent Fourier transform. The configuration of the simulations is as follows: a short pulse of linearly polarized light is sent perpendicularly to the surface of the heterostructure from a source placed above the metal. Placing different monitors in several spots we have measured certain physical properties, such as transmission, reflection or electric field intensity and distribution, which bring us information about the system response. Thanks to the periodic boundary conditions of the axes that form the plane where the layers are contained we have only had to introduce a single unit cell of the lattice.

In our simulations, data from Palik were used for the permittivity of SiO_2 [7], and from Johnson and Christy for the Au [8].

The heterostructure used throughout the project is formed by a Au layer of 30 nm and underneath a dielectric one of 600 nm, both in thickness. These dimensional parameters have been chosen in order to have suitable values when it comes to the applications and the design of a real device. The honeycomb lattice is the periodic

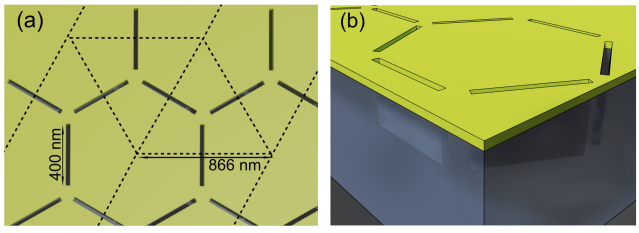

FIG. 2: Top (a) and 3D (b) views of the heterostructure with honeycomb lattice of 400 nm long and 30 nm wide bars. The unit cell is represented in dashed line.

structure chosen and it is formed by rectangular empty bars of 400 nm in length and 30 nm in width which are carved in both Au and dielectric layers. The carving is such that it always crosses the Au layer and the depth

in the dielectric material will be optimized as explained later.

The whole heterostructure is surrounded by air. This way, the air that fills the carved holes together with the dielectric material of the bottom layer forms a two-dimensional photonic crystal.

The associated Bravais lattice is a hexagonal one (shown in Fig. 2(a) by the regular rhombus in dashed line) whose atomic base contains two non-equivalent knots of the hexagons. The diffraction peaks of the knot-line families are ordered according to the decreasing distance d of two adjacent lines in each family. We work with a honeycomb lattice with a distance between the nearest neighbor hexagons (pitch) of $a = 866$ nm. Therefore, for this structure, the diffraction condition for the most separated line family corresponds to $\lambda = a\cos(\frac{\pi}{6}) = 749.9$ nm. This result should be compared with the corresponding absorption peak in the spectrum shown in Fig. 3(a) that was obtained by numerical simulation. As we can observe, this absorption peak appears slightly shifted in comparison with the expected value. This can be explained because the effective value of the refractive index is slightly larger than the unity owing to the presence of the underneath dielectric layer.

It can also be observed that the wavelengths corresponding to the maximum and minimum of the transmission and reflection functions are not exactly in the same position. This is because each extremum corresponds to each of the two standing-wave solutions that accumulate the energy of the electric field in two different regions: one in the metal, giving rise to a collective absorption mode, and the other outside the metal, producing a bright mode of reflection.

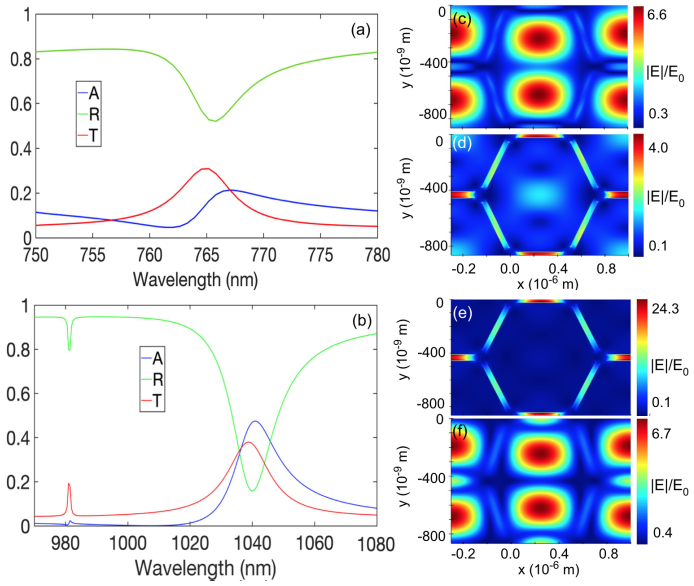

FIG. 3: Panels (a) and (b) show the reflection, transmission, and absorption spectra around the position of the diffraction peaks corresponding to the two metal-dielectric interfaces (with the air and the SiO_2). At the two peak wavelengths (765 nm and 1038 nm), panels (c) and (f) show the electric field modulus inside the air (5 nm above the Au layer) and the SiO_2 layer (5 nm below the Au layer), respectively. Panels (d) and (e) show the electric field modulus measured exactly in the middle of the Au layer at the same two wavelengths, respectively.

III. RESULTS

So as to obtain an overview of the behavior of our heterostructure when electromagnetic radiation reaches it, the first results to comment (and from which we will make subsequent simulations varying certain parameters) is presented in Fig. 3 where we plot the transmission, reflection, and absorption spectra as a function of the incident wavelength for two regions of interest obtained by numerical simulation as described in the previous section. We have used SiO_2 for the substrate and a depth of the trenches on the SiO_2 layer of 100 nm. Absorption can be obtained from $A = 1 - T - R$ where T and R are the transmission and the reflection functions, respectively.

We have already discussed that those peaks that interest us for our sensing application are the diffraction ones that correspond to absorption peaks, and whose electric field excitation modes go out of the heterostructure.

The first one, located at 765 nm, corresponds to the peak generated by the diffraction condition between the top interface of the metal and the air ($n = 1$) whose position has already been calculated in the previous section. Figure 3(c) shows an extended electric field enhancement in the air region that is almost perpendicular to the surface of the metal and achieves a maximum value of about 6.6 times that of the impinging radiation. This electric-field enhancement is intensified owing to the confinement effect caused by the photonic crystal. Interestingly, there is a second diffraction peak around 1038 nm for which the field distribution presents a high electric field density in the SiO_2 region (Fig. 3(f)). It is also shifted to the infrared since the effective refractive index is close to that of the silica. This peak should be found at $749.9 \times 1.5 = 1124.9$ nm if the value of the effective refractive index was exactly 1.5 (value of n for the silica).

Therefore, the role of the photonic crystal is to favor, in each of the diffraction peaks with the two interfaces, that the effective refractive index is close to that of each dielectric material (air and SiO_2), splitting even more the two diffraction modes. Later we will see that this property is essential in order to get a high sensitivity in the sensing application.

It is worth commenting that the sharp absorption peak that appears near 970 nm is an excitation mode associated only with the photonic crystal since almost no excitation is observed within the metal.

One of the parameters that conditions the diffraction peak intensities we want to study is the depth of the trenches etched on the dielectric material. In essence, this will vary the photonic crystal thickness with which the electromagnetic wave interacts, resulting in greater or

lesser enhancement of the confinement effect at the metal interfaces. Therefore, we made the comparative study for different trenches depths which is shown in Fig. 4.

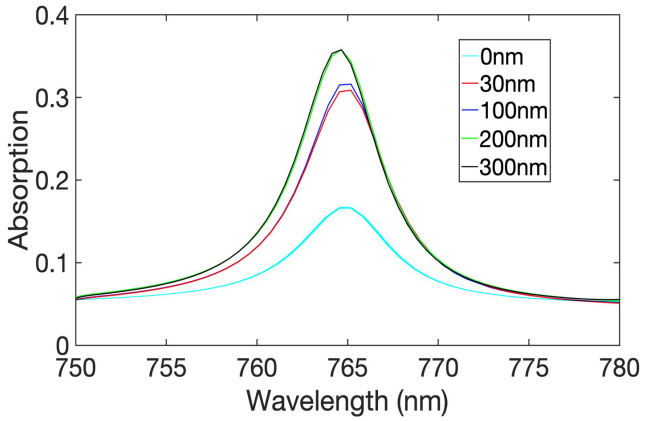

FIG. 4: Absorption spectra around the peak associated with the air diffraction obtained, with SiO_2 as dielectric material and as a function of the depht of the trenches. Note the low intensity of the peak when the depth of the trenches is zero and the photonic crystal is not present.

Should the width of the photonic crystal be much smaller than the wavelength, the incident photons will not interact with the crystal. Once we find the minimum depth of the trenches for the crystal to interact with the impinging light, no matter how much we increase this depth, we will not obtain a much better result in terms of absorption peak intensity.

Taking into account that the absorption peak broadens above 100 nm we decided to proceed with the simulations associated with the sensor itself with a heterostructure where the trenches are carved 100 nm into the SiO_2 layer.

In this sensing application we put the material to detect above the Au layer, causing both diffraction peaks will be affected. However, the air excitation peak will undergo a much more intense shift, as this is the mode that interacts most with the new material introduced. So the objective of our system will be to measure the splitting between the two diffraction peaks and compare their positions when different refractive-index materials are placed above the structure. Therefore, Fig. 3 shows the reference case where the material to be sensed has $n = 1$ as a refractive index (air). In this case, we have the maximum distance between the two diffraction peaks whose positions have already been calculated and appears at $\lambda_1 = 765$ nm and $\lambda_2 = 1038$ nm.

In order to model the spectrum behavior when a new material with $n > 1$ is introduced, we run simulations with a 50 nm thick layer of this new dielectric material above our heterostructure. With the aim of analyze different possible materials to be detected, different values for the refractive index of the new dielectric material layer have been used: $n = 1.1, 1.2, 1.3, 1.4$. This test layer could represent the presence of different materials we want to detect like molecules, viruses or antibodies.

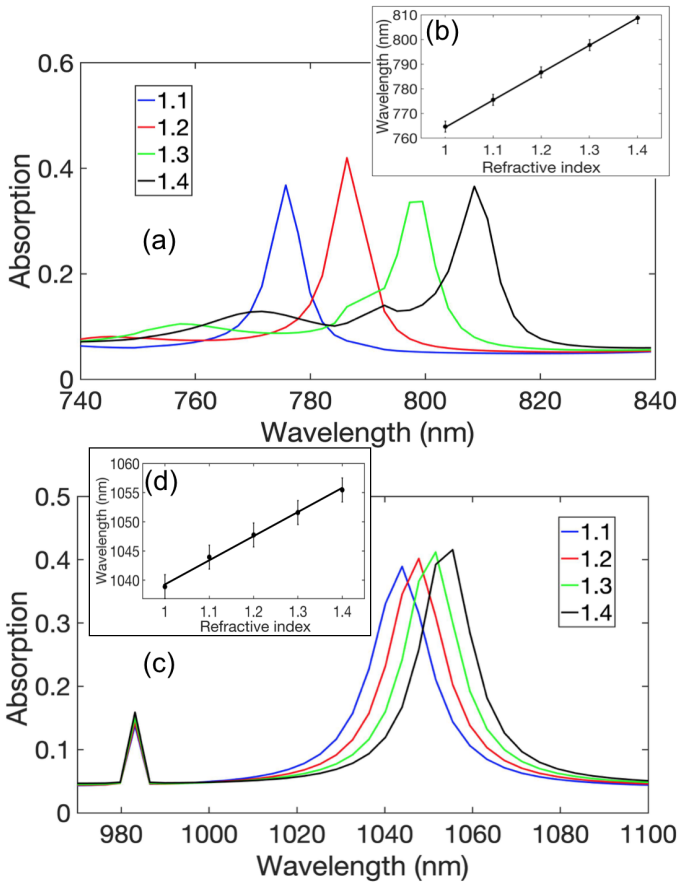

FIG. 5: Absorption spectrum for each refractive index material over the structure for trenches of 100 nm in depth carved through the SiO_2. Panel (a) and (c) correspond to the first and second absorption peaks studied before, respectively. Panels (b) and (d) show the wavelength in which the peak appears as a function of the refractive index and their respective regression line $y_1 = 108.62x + 656.24$ nm and $y_2 = 41.57x + 997.55$ nm

This way, increasing the refractive index of the layer, both the peak generated from the diffraction condition with the interface between this new layer and the Au layers (Fig. 5(a)) and the peak from the interface between the Au and the SiO_2 layers (Fig. 5(c)) are clearly linearly shifted to higher wavelengths thus moving away from the reference case. So as the refractive index of the sense layer raises, the first diffraction mode becomes less energetic and shifts towards the infrared.

On the other hand, the non n-dependence of the absorption peak appearing around 970 nm confirms that it is a pure photonic crystal excitation.

Therefore, the sensor sensitivity for the detection of changes in the refractive index of the sensing layer can be obtained for both diffraction peaks from the slopes in Fig. 5(b) and Fig. 5(d): $S_1 = 108.6$ nm/RIU and $S_2 = 41.6$ nm/RIU (RIU: refractive index unit).

As we have already discussed, the first diffraction peak (between the sensing layer and the Au layer) is notice-

ably more sensitive to reffractive-index variations. These sensitivity values must be normalized to the width of the peak at mid-height in order to enable the direct comparison with other results in the literature. Specifically, for the first peak we have a figure of merit (FOM) of 22.1/RIU. The role of the photonic crystal is vital to obtain such a high value in the sensitivity since thanks to its interaction, the two diffraction peaks are markedly splitted in wavelength. So this obtained sensitivity is more than competitive in comparison with other plasmonic sensors in recent publications [9-10], in which the obtained values for the FOM are around 4/RIU.

Once we have designed and analyzed our sensing structure, we can try to improve even more its sensitivity. A greater splitting in wavelength between the air-metal and the metal-dielectric diffraction peaks would lead to a higher sensitivity sensor, since the absorption peaks will have a wider range of variation when introducing the new material above the structure.

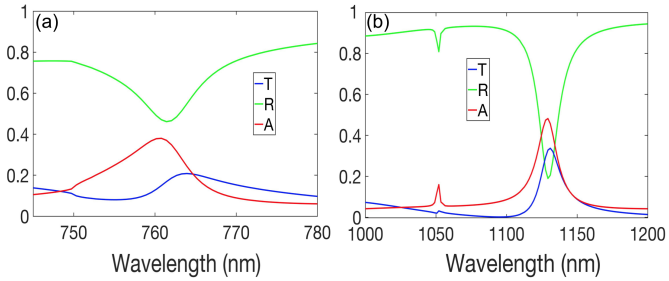

FIG. 6: Absorption, transmission, and reflection spectra in the interface between the air and the Au layer (a), and between the Au and the (n=2)-material layers (b).

Therefore, we run a simulation where the SiO_2 layer used throughout the project was replaced by a $n = 2$ material one with exactly the same geometric features. In this situation, the diffraction peaks are even more splitted and intense since now we have built a more efficient photonic crystal that generates a greater enhancement of the plasmonic excitations.

It is worth observing that the peak associated with the diffraction condition in the air-metal interface appears practically in the same position as it did for the SiO_2 since nothing has changed near this interface. However, the diffraction peak between the Au layer and the dielectric material of $n = 2$, depicted in Fig. 6(b), appears at 1130 nm, which provides a wider range of variation of the air-metal diffraction peak.

However, for the complete study of the sensor, SiO_2 has been used as a dielectric since it is a standard material easy to combine with Au to manufacture the heterostructure by lithographic techniques.

IV. CONCLUSIONS

The area of plasmonics and photonics has a plethora of applications. We have already seen that one of them is the development of detection devices. In our case, we have characterized the optical response of a heterostructure basically formed by Au and SiO_2 layers patterned with a honeycomb lattice with the aim of simulating the behavior of a sensor of refractive index changes. The TDTD method has been our working tool when it comes to these simulations. The role of the photonic crystal has been fundamental to get an enhancement of the electric field enough to obtain an optimal response as well as the tuning of other parameters to achieve the highest efficiency. In this way, we have obtained a sensitivity of 22.1/RIU, a much higher value than that achieved in other sensors with similar characteristics.

Acknowledgments

A heartfelt thanks to my advisor Amílcar Labarta, without his dedication and passion, this project would not be possible. Thanks also to Javier Rodríguez for introducing me to the world of Lumerical and its applications. Many thanks to my parents for supporting me in each of my life's decisions. And last, but not least, special thanks to my degree colleagues.

[1] Maier, S. *Plasmonics: Fundamentals and Applications.* Springer (2007).
[2] Novotny, L. and Hecht, B. *Surface plasmons. In Principles of Nano-Optics* (pp. 378-418). Cambridge University Press (2006).
[3] Kravets, V., Kabashin, A., Barnes, W., and Grigorenko, A. *Plasmonic Surface Lattice Resonances: A Review of Properties and Applications.* Chemical Reviews, 118, 5912-5951 (2018).
[4] Conde-Rubio, A., Rodríguez, A. F., Espinha, A., Mihi, A., Pérez-Murano, F., Batlle, X., and Labarta, A. *Geometric frustration in ordered lattices of plasmonic nanoelements.* Scientific Reports, 9(1), 1-10 (2019).
[5] Halas, N. *Nanophotonics: an overview.* Materials Today, 7, 49 (2004).
[6] Lumerical Inc. https://www.lumerical.com/products/
[7] Palik, E. D. (Ed.). *Handbook of optical constants of solids.* (vol.3). Academic Press (1998).
[8] Johnson, P. B. and Christy, R. W. *Optical constants of the noble metals.* Physical Review B, 6(12), 4370 (1972).
[9] Becker, J., Trügler, A., Jakab, A. et al. *The Optimal Aspect Ratio of Gold Nanorods for Plasmonic Bio-sensing.* Plasmonics 5, 161–167 (2010).
[10] Henzie, J., Lee, M. H., and Odom, T. W. *Multiscale patterning of plasmonic metamaterials.* Nature Nanotechnology, 2(9), 549-554 (2007).

APPENDIX

Throughout the study, the recurrent use of simulations to obtain the behavior of the system in different situations is mentioned. Although the mathematical operation of the software we work with has already been explained, it is important to highlight its learning and use process.

To simulate the behavior of our system in Lumerical, we build the heterostructure graphically, adding each element that forms it and characterizing it with the corresponding geometric parameters.

Once the structure was assembled, a radiation source, whose properties are also set by us, is added. In order to take measures of different physical properties, we make use of several monitors placed in different interest spots. It has already been mentioned that Lumerical works with a finite set of points, so once the setup is configured, we can vary the mesh of our simulation so that we change the number of points of space in which the software will solve Maxwell's equations. Due to the complexity of the simulations, they usually take days to finish.

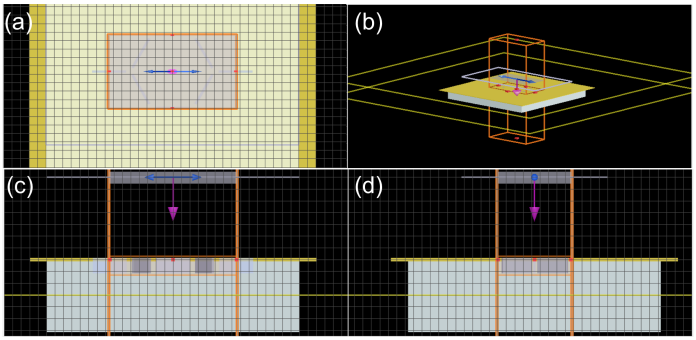

FIG. 7: Panels (a), (b), (c), and (d) show XY, perspective, XZ, and YZ Lumerical views, respectively of the heterostrucutre we have simulated. The source, the mesh, and the monitors are also depicted.